the plant journal

SEB SOCIETY FOR EXPERIMENTAL BIOLOGY

The Plant Journal (2021) doi: 10.1111/tpj.15620

Hydroxycinnamic acid-modified xylan side chains and their cross-linking products in rice cell walls are reduced in the *Xylosyl arabinosyl substitution of xylan 1* mutant

Carolina Feijao[1,†], Kris Morreel[2,3,†], Nadine Anders[1], Theodora Tryfona[1], Marta Busse-Wicher[1], Toshihisa Kotake[1,4], Wout Boerjan[2,3,*] and Paul Dupree[1,*]

[1]*Department of Biochemistry, University of Cambridge, Tennis Court Road, Cambridge CB2 1QW, UK,*
[2]*Department of Plant Biotechnology and Bioinformatics, Ghent University, Technologiepark 71, Ghent 9052, Belgium,*
[3]*VIB Center for Plant Systems Biology, Technologiepark 71, Ghent 9052, Belgium, and*
[4]*Saitama University, 255 Shimo-Okubo, Saitama 338-8570, Japan*

Received 22 May 2021; revised 13 November 2021; accepted 29 November 2021.
*For correspondence (e-mails pd101@cam.ac.uk; wout.boerjan@psb.vib-ugent.be).
†These authors contributed equally to this work.

SUMMARY

The intricate architecture of cell walls and the complex cross-linking of their components hinders some industrial and agricultural applications of plant biomass. Xylan is a key structural element of grass cell walls, closely interacting with other cell wall components such as cellulose and lignin. The main branching points of grass xylan, 3-linked L-arabinosyl substitutions, can be modified by ferulic acid (a hydroxycinnamic acid), which cross-links xylan to other xylan chains and lignin. XAX1 (Xylosyl arabinosyl substitution of xylan 1), a rice (*Oryza sativa*) member of the glycosyltransferase family GT61, has been described to add xylosyl residues to arabinosyl substitutions modified by ferulic acid. In this study, we characterize hydroxycinnamic acid-decorated arabinosyl substitutions present on rice xylan and their cross-linking, in order to decipher the role of XAX1 in xylan synthesis. Our results show a general reduction of hydroxycinnamic acid-modified 3-linked arabinosyl substitutions in *xax1* mutant rice regardless of their modification with a xylosyl residue. Moreover, structures resembling the direct cross-link between xylan and lignin (ferulated arabinosyl substitutions bound to lignin monomers and dimers), together with diferulates known to cross-link xylan, are strongly reduced in *xax1*. Interestingly, apart from feruloyl and *p*-coumaroyl modifications on arabinose, putative caffeoyl and oxalyl modifications were characterized, which were also reduced in *xax1*. Our results suggest an alternative function of XAX1 in the transfer of hydroxycinnamic acid-modified arabinosyl substitutions to xylan, rather than xylosyl transfer to arabinosyl substitutions. Ultimately, XAX1 plays a fundamental role in cross-linking, providing a potential target for the improvement of use of grass biomass.

Keywords: arabinosyltransferase, Glycosyltransferase family 61, hydroxycinnamic acid, lignin, *Oryza sativa*, xylan, xylosyl arabinosyl substitution of xylan 1.

INTRODUCTION

Grass cell walls are an abundant and renewable source of energy-rich polymers for a great variety of industrial applications ranging from animal nutrition to the production of second-generation biofuels. A major constraint in the industrial use of grass cell walls lies in their recalcitrance to breakdown due to the complexity associated with the arrangement and interactions of cell wall components (Abramson et al., 2010; Bhatia et al., 2017; Pauly and Keegstra, 2008). The composition and cross-linking of cell wall components differs greatly from that in eudicot cell walls (Hatfield et al., 2016; Vogel, 2008).

In general, plant cell walls are composed of a scaffold of cellulose microfibrils embedded in a matrix containing a mixture of hemicelluloses, pectins, and structural proteins, and in some instances non-polysaccharide, non-protein components such as lignin. In grasses, xylan is the main hemicellulosic polysaccharide in the cell wall. Xylan consists of a backbone of β-(1,4)-linked D-xylopyranosyl (X) sugars, which can be decorated with sugar side chains and acetyl groups (Ebringerova et al., 2005). The most abundant sugar side chains of xylan in grasses are α-(1,3)-linked L-arabinofuranosyl (A) residues, which can be decorated at their O-5 position with

hydroxycinnamic acids like ferulic acid (FA) and *p*-coumaric acid (*p*CA) through an ester linkage (Hatfield et al., 2016). Specifically, FA has been described to cross-link xylan chains through oxidative coupling with other FA groups (Ishii, 1997). 5–5-, 8–O–4-, 8–5-, and 8–8-coupled ferulate dehydrodimers as well as dehydrotrimers and -tetramers have been identified (Bento-Silva et al., 2018; Burr and Fry, 2009; Ralph, 2010; Waterstraat and Bunzel, 2018). The diversity of coupling products highlights that these ferulate structures are synthesized in a combinatorial radical cross-coupling process similar to that which occurs during lignification (Ralph, 2010; Ralph et al., 2004). Lignification results from the polymerization of the monolignols *p*-coumaroyl, coniferyl, and sinapyl alcohol, yielding the *p*-hydroxyphenyl (H), guaiacyl (G), and syringyl (S) units in lignin (Freudenberg and Neish, 1968; Ralph et al., 2019; Vanholme et al., 2019). In the oxidative environment of the cell wall, peroxidase-catalyzed oxidation of ferulates and lignin units and monomers and their subsequent radical–radical cross-coupling is expected and this idea is supported by biomimetic co-polymerization of ferulates into synthetic lignins (Grabber et al., 1995, 2000; Quideau and Ralph, 1997; Ralph et al., 1992). Many of the resulting cross-coupling units were indeed identified in lignin (Bunzel et al., 2004; Jacquet et al., 1995; Ralph et al., 1995). Because ferulates in monocot cell walls are mostly present as FA-modified α-L-arabinofuranosyl (5-O-feruloyl arabinose; FA-A) residues (1,3)-linked to the backbone (Ishii, 1997), it is generally accepted that these latter ferulates are involved in the lignin–polysaccharide connections (Grabber et al., 2002). This has been recently supported by the detection of the cross-coupling products of either coniferyl or sinapyl alcohol with FA-A in hydrolysis extracts of *Miscanthus* and maize (*Zea mays*) lignified cell walls (Lapierre et al., 2019). Cross-linking of lignin and xylan through FA is seen as a key element in enhancing the structural complexity and recalcitrance of the cell wall to breakdown (Buanafina, 2009; de Oliveira et al., 2015; Terrett and Dupree, 2018). In some instances, FA-A can adopt more complex forms when decorated with additional sugars such as β-(1,2)-linked xylopyranosyl (X), which leads, e.g., to the formation of X-(FA)-A (2-O-xylopyranosyl-(5-O-feruloyl) arabinose) or the α-(1,2)-linked L-galactopyranosyl modification of X-(FA)-A (Allerdings et al., 2006; Saulnier et al., 1995; Schendel et al., 2015; Wende and Fry, 1997). However, the function of the additional sugar modifications is unknown. Quantitative analysis of side chains in *Miscanthus* xylan showed that X-A substitutions are rare with a frequency of 1–2% in leaves and considerably less in stem; similar substitution profiles were seen in rice (*Oryza sativa*) leaves (Tryfona et al., 2019). In contrast to FA, the combinatorial radical cross-coupling of *p*CA or *p*CA esters, resulting in lignin–hemicellulose connections and *p*CA dimers, cross-linking polysaccharide chains have not been reported *in planta* (Ralph, 2010), although *p*CA can be involved in photo-induced formation of cyclodimers with FA (Ford and Hartley, 1989, 1990).

Because FA modifications occur on A side chains of xylan, A side chains are fundamental for the cross-linking of cell wall components. Members of the CAZY family GT61 have been described as α-1,3-arabinosyltransferases adding A side chains to the xylan backbone (Anders et al., 2012; Zhong et al., 2018), while others were described as β-1,2-xylosyltransferases for xylan (Chiniquy et al., 2012; Voiniciuc et al., 2015; Zhong et al., 2018) or for N-glycans (Bencur et al., 2005). Xylan arabinosyltransferases *Ta*XAT1, *Ta*XAT2, *Os*XAT2, and *Os*XAT3 add α-(1,3)-A side chains to xylan *in planta* and this catalytic activity has been confirmed for *Os*XAT2 in *in vitro* assays and for its homolog in *Sorghum* (Anders et al., 2012; Shao et al., 2020; Zhong et al., 2018). Interestingly, analysis of water-extractable xylan from wheat (*Triticum aestivum*) flour showed that the reduction of α-(1,3)-A in *Ta*XAT1 RNA interference lines is accompanied by a reduction of bound FA (Freeman et al., 2017). A significant reduction in FA and *p*CA released upon base hydrolysis, along with enhanced saccharification, was also reported in *xax1*. In contrast to other GT61 xylan β-1,2-xylosyltransferases, XAX1 has been inferred to act on A side chains rather than the xylan backbone forming β-(1,2)-xylopyranosyl-α-(1,3)-arabinofuranosyl (X-A) side chains (Chiniquy et al., 2012), but it is unclear how changes in a minor side chain substitution result in a large decrease of bound FA and *p*CA.

Here, we investigated the significance of XAX1 in hydroxycinnamic acid modification of xylan and its impact on cross-linking. We established polysaccharide analysis by carbohydrate gel electrophoresis (PACE) and applied liquid chromatography–mass spectrometry (LC-MS) as methods for analyzing hydroxycinnamic acid-modified xylan oligosaccharides of wild-type (WT) rice mature leaves. We then compared their abundance in WT to that in the *xax1* mutant. Our analysis showed that not only the X-(FA)-A structure was reduced in *xax1*, but surprisingly also hydroxycinnamic acid-decorated side chains which were not modified by a xylosyl residue like FA-A and *p*CA-modified α-L-arabinofuranosyl (5-O-*p*-coumaroyl arabinose; *p*CA-A) residues (for reference, Figure 1 shows the main structures and abbreviations used in this manuscript of the most abundant hydroxycinnamoyl-modified A structures found in the LC-MS analysis). This finding could be explained by XAX1 acting as hydroxycinnamoyl α-1,3-arabinosyltransferase rather than β-1,2-xylosyltransferase. The observed changes in xylan side chain abundance in *xax1* lead to a plethora of downstream changes in plant cell wall cross-linking, namely a reduction of diverse hydroxycinnamate–hydroxycinnamate and monolignol–hydroxycinnamate coupling products.

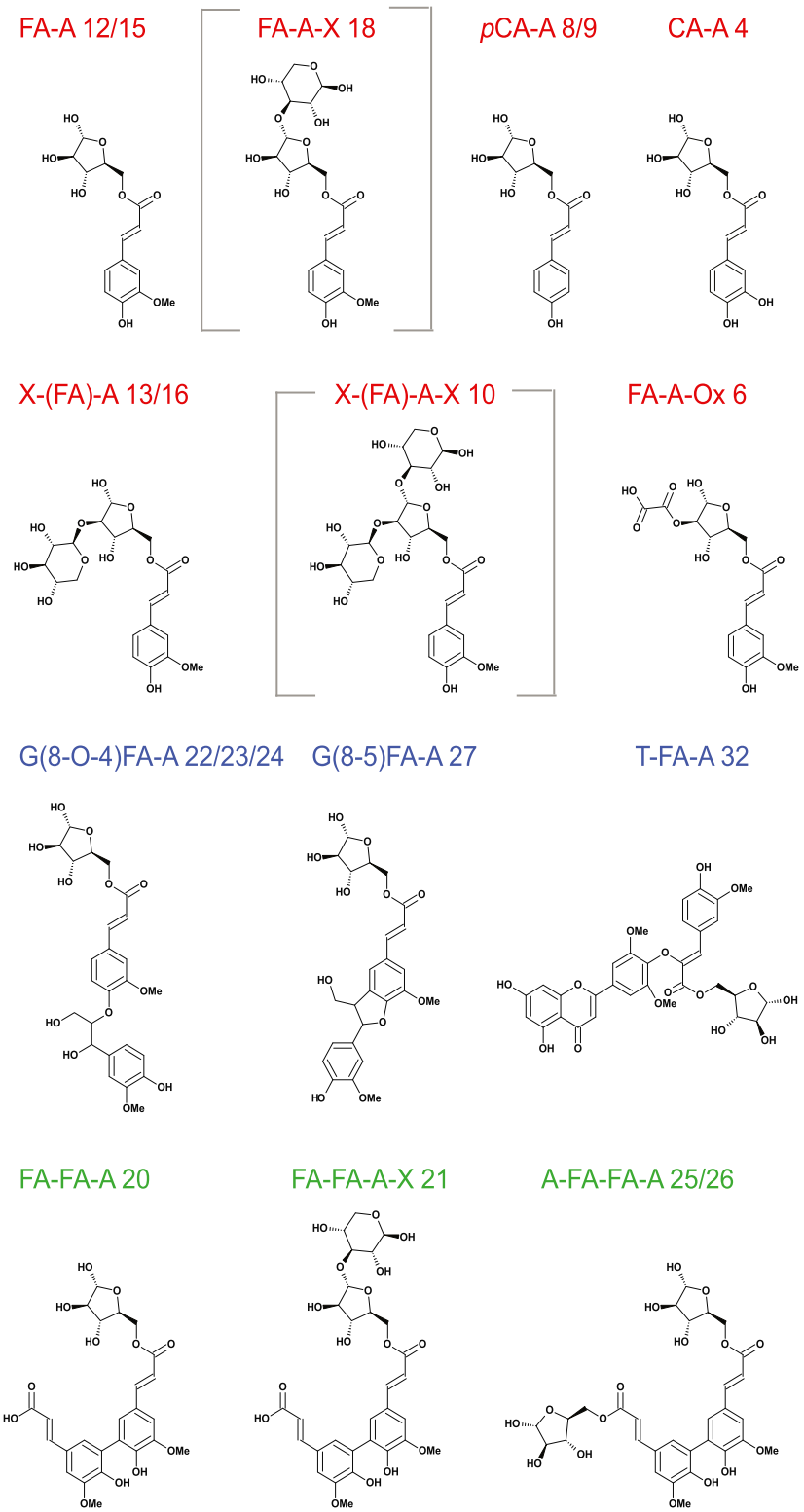

Figure 1. Abbreviations used in this study with their corresponding chemical structures, confidently assigned by MS^n fragmentation in the phenolic profiling. Linkages in ferulate dimers are tentatively shown as 5–5, but 8–8, 8–O–4, or 8–5 linkages are equally likely. Compounds classified as hydroxycinnamic acid-modified A are shown in *red*, xylan cross-linking moieties in *green*, and xylan–lignin cross-linking moieties in *blue*; see Table S2 for trivial names and further information. Boxed-in structures contain a xylose residue from the xylan backbone.

RESULTS

PACE as a method to detect hydroxycinnamic acid-decorated xylan side chains

To analyze hydroxycinnamic acid modification of xylan in an easy and robust way, we first established PACE as a method using WT rice. Xylan substitutions decorated with hydroxycinnamic acid can be analyzed using mild trifluoroacetic acid (TFA) hydrolysis (Bowman et al., 2011; Saulnier et al., 1995; Wende and Fry, 1997). Mild TFA treatment leads to the preferential cleavage of arabinofuranosyl linkages over cleavage of the xylose backbone, removing A side chains from the xylan backbone, while largely preserving the ester-linked hydroxycinnamic acid decorations on A side chains. Alcohol-insoluble residue (AIR) from mature rice leaves, the tissue in which changes in *xax1* were originally reported (Chiniquy et al., 2012), was analyzed in a time course of 0–100 min of mild TFA hydrolysis. To identify structures harboring the alkali-sensitive ester-linked hydroxycinnamic acid groups on A, TFA hydrolysis was followed by NaOH treatment. This treatment also removes acetyl groups present in rice xylan (Gao et al., 2017); however, removal of acetyl groups on xylan oligosaccharides results only in minor changes to the band positioning in PACE (Busse-Wicher et al., 2014).

As expected, mild TFA hydrolysis leads to the immediate release of large amounts of arabinose, co-migrating with the xylose (X_1) standard in the PACE gel (Figure 2). Following 60 min of TFA hydrolysis, a ladder of NaOH-resistant oligosaccharides (presumably hydrolysis products of the xylan backbone) are observed, which co-migrate with the xylooligosaccharide standard X_1 to X_6. Most importantly, from 60 min of hydrolysis time onwards, at least three major bands were apparent, which did not co-migrate with the xylooligosaccharide standard and were sensitive to NaOH treatment (Figure 2), suggesting the detection of hydroxycinnamic acid-modified A side chains by PACE.

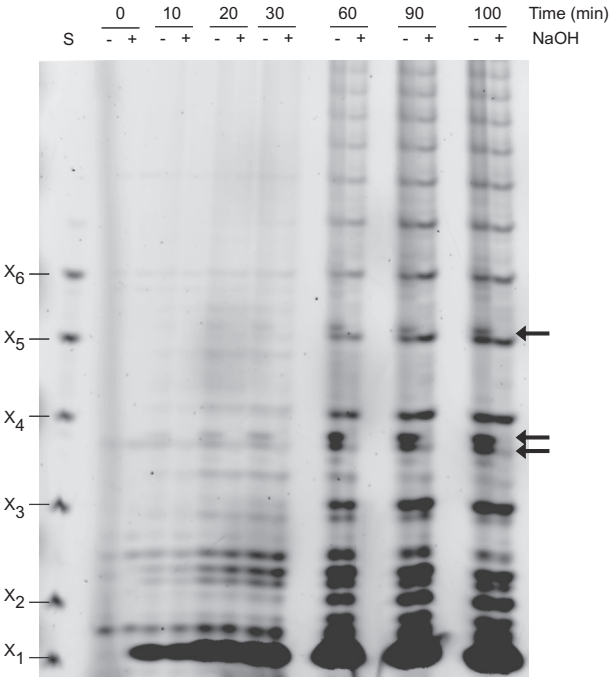

Figure 2. Identification of NaOH-sensitive xylan hydrolysis products by PACE. PACE analysis of mild TFA hydrolysis products from rice leaf AIR at successive time points of hydrolysis (0–100 min). The hydrolysates were tested for the presence of ester-linked groups by comparing hydrolysis profiles in the absence (–) or presence (+) of NaOH. NaOH-sensitive bands are marked with an arrow. S: xylooligosaccharide standard X_1–X_6. Note that the accumulation of NaOH-resistant bands below X_3 that do not align with the xylooligosaccharide standard are most likely small non-xylan oligosaccharides released during TFA hydrolysis.

Identification of feruloyl and *p*-coumaroyl-modified A side chains

To characterize the NaOH-sensitive structures, TFA hydrolysates were subjected to solid phase extraction (SPE) using C18 as stationary phase and elution with different ethanol concentrations and the fractions were analyzed by PACE (Figure 3). While the xylooligosaccharide ladder obtained from TFA hydrolysis elutes with 10% ethanol (Figure S1), the NaOH-sensitive bands eluted at ethanol percentages of 15–18%, indicating greater hydrophobicity. Fractions harboring the hydroxycinnamic acid-modified structures were selected for derivatization with procainamide hydrochloride (217 Da) and analyzed by matrix-assisted laser desorption ionization (MALDI)-MS. MALDI-MS analysis allowed the detection of masses corresponding to procainamide hydrochloride-modified *p*-coumaroyl pentose (*m*/*z* 514 Da), feruloyl pentose (*m*/*z* 544 Da), and feruloyl dipentose (*m*/*z* 676 Da), as well as small amounts of *p*-coumaroyl dipentose (*m*/*z* 646 Da) (Figure 3). Monosaccharide analysis of the 100% ethanol SPE eluate showed the presence of arabinose and xylose (Table S1). These data together with the published data on rice xylan structure and the reported effect of TFA hydrolysis on xylan led to the assignment of *p*-coumaroyl pentose as *p*CA-A, feruloyl pentose as FA-A, *p*-coumaroyl dipentose as X-(*p*CA)-A (2-O-xylopyranosyl-(5-O-*p*-coumaroyl) arabinose), and feruloyl dipentose as X-(FA)-A.

While MALDI is not a quantitative technique *per se*, it provides reproducible ratios between the peak intensities, allowing the assessment of relative quantities (Lerouxel et al., 2002). By comparing the relative peak intensities of the MALDI spectra of the four assigned structures in a specific fraction (Figure 3(a–d)) with the relative band intensities of the NaOH-sensitive bands of the correlating fractions in the PACE gel (Figure 3(e)), the NaOH-sensitive structures in the PACE gel can be assigned. FA-A and *p*CA-A migrate as doublet, which is indicative of their similarity in size and properties with *p*CA-A running slightly quicker in the PACE analysis. This is consistent with *p*CA-A eluting

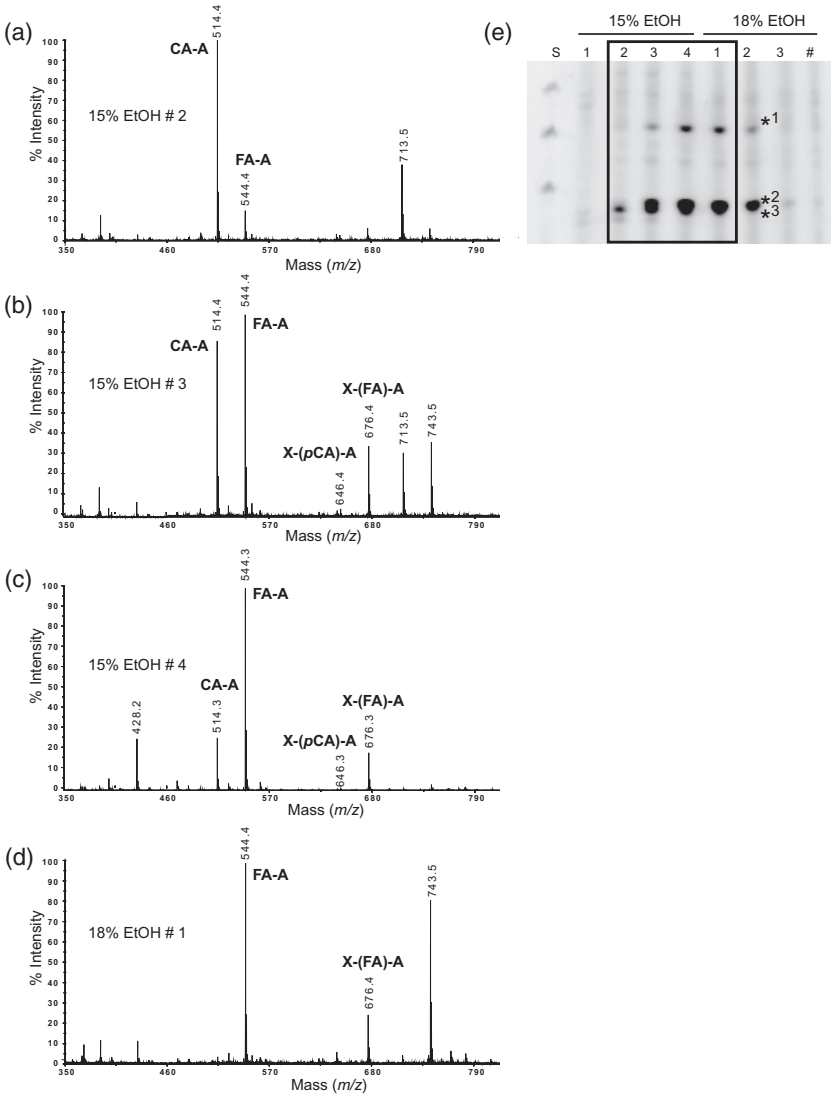

Figure 3. Characterization of NaOH-sensitive xylan hydrolysis products by MALDI-MS. MALDI spectrum showing the mass (*m*/*z*) of TFA hydrolysis products obtained from different fractions of ethanol (EtOH) eluates. (a) Fraction #2, (b) fraction #3, and (c) fraction #4 of the 15% ethanol elution and (d) fraction #1 of the 18% ethanol elution. Note that the identity of the peaks of 713.5 and 743.5 Da is unclear, but may correspond to doubly derivatized anhydrocoumaroyl and -feruloyl pentose, respectively. (e) PACE analysis of NaOH-sensitive xylan hydrolysis products of fractions of the SPE eluate. Four fractions (#1–4) were collected after elution with increasing ethanol percentages (15 and 18%). Boxed fractions were analyzed by MALDI-MS (a–d). Asterisk 1: X-(FA)-A, asterisk 2: FA-A, and asterisk 3: *p*CA-A. S: xylooligosaccharide standard X_6–X_4 (top to bottom). Note the change of relative abundance of *p*CA-A, FA-A, and X-(FA)-A in the different fractions.

slightly before FA-A in the ethanol elution. The further modified X-(FA)-A band runs significantly more slowly in the PACE gel, while the low-abundance X-(*p*CA)-A could not be robustly detected by PACE. To support further the assignment of hydroxycinammic acid structures by PACE, the 100% ethanol SPE eluate was digested with a GH3 β-xylosidase from *Chaetomium globosum* (*Cg*GH3), which has been found to cleave β-(1,2)-linked xylose side chains (Tryfona et al., 2019). Of the three assigned NaOH-sensitive structures X-(FA)-A, FA-A, and *p*CA-A, only X-(FA)-A was sensitive to hydrolysis with GH3 xylosidase (Figure S1), confirming its assignment.

Not only X-(FA)-A, but also FA-A and *p*CA-A xylan side chains are reduced in *xax1*

Chiniquy et al. (2012) reported that bound FA and *p*CA were approximately halved in the plant cell wall of mature rice leaves in *xax1*. To analyze how the reduction of FA and *p*CA relates to modification of the specific xylan side chains, i.e., A and X-A, quantitative changes of hydroxycinnamic acid-modified structures in WT and *xax1* mutant rice were analyzed. AIR of mature leaves was subjected to mild TFA hydrolysis and analyzed by PACE, as established above, and the signal intensity of relevant bands was quantified. Four different time points of hydrolysis (180, 240, 330, and 450 min) were used to ensure that the comparison of WT and *xax1* is not compromised by different rates of release and degradation of the structures of interest, particularly given that *xax1* is reported to show increased extractability of sugars (Chiniquy et al., 2012). Consistent with the findings of Chiniquy et al. showing the loss of X-A side chains, X-(FA)-A is strongly reduced in *xax1* (Figure 4). FA-A and *p*CA-A could not be completely separated using PACE to quantify the bands separately; however, quantification of both bands together revealed a combined reduction in *xax1* compared to WT. This

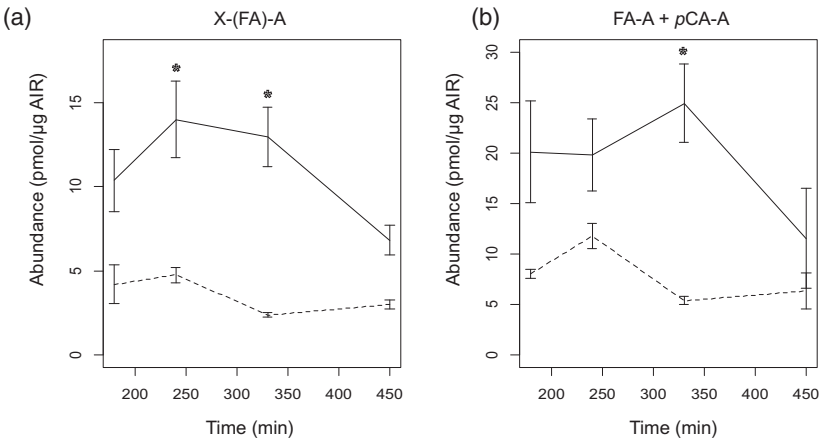

Figure 4. Hydroxycinnamic acid-modified arabinose structures are reduced in *xax1*. Quantification of PACE bands corresponding to (a) X-(FA)-A and (b) FA-A and *p*CA-A. Three biological replicates of WT and *xax1* leaf AIR were TFA-hydrolyzed for 180, 240, 330, and 450 min, and the SPE eluate was analyzed by PACE. Solid line: WT, dashed line: *xax1*. Asterisks mark significant differences as determined by the Student *t*-test ($P < 0.05$).

reduction of FA-A and *p*CA-A cannot be easily explained as a direct effect of the proposed XAX1 β-1,2-xylosyltransferase activity.

Complexity of hydroxycinnamic acid structures in WT and *xax1* mutant rice

To achieve better resolution of the different hydroxycinnamic acid-modified xylan side chains and to analyze the downstream effects of the change in xylan structure on the cross-linking of xylan and lignin in the plant cell wall, hydroxycinnamic acid structures obtained from mild TFA hydrolysis of WT and *xax1* AIR were analyzed using ultrahigh-performance LC (UHPLC) hyphenated to a Fourier transform ion cyclotron resonance mass spectrometer (FTICR-MS; Figure 5(a)). This allowed the profiling of up to 6008 compounds (see Experimental Procedures). Some of the compounds were structurally assigned using accurate mass (*m*/*z*) determination and MS^n spectral elucidation (see Experimental Procedures). This led to the highly confident structural characterization of 32 of the most abundant compounds (Figure 1, Tables 1 and S2). Although MS^n data provided strong evidence for the structures of the 32 compounds, their full authentication needs either purification for NMR or chemical synthesis of reference compounds. In addition, based on the structures of these 32 compounds, the phenolic profiles were searched for masses corresponding to isomers and alternative structures that were assumed to be present (see Experimental Procedures). This yielded a list of 60 features of which the chemical formulae matched the mass of those searched structures (Table S2). However, as MS^n spectra were absent or of low quality, these 60 features could be only tentatively assigned. Below, the 32 confidently characterized compounds are referred to by a shorthand name and a bold number, whereas only a shorthand name is mentioned for each of the 60 tentative compounds.

To unravel the differences in the cell wall phenolic profiles of WT and the *xax1* mutant, the compound abundances were subjected to piecewise regression modeling including the genotype (WT versus *xax1* mutants) and hydrolysis time, and their interaction as factors as shown in Figure 5(b); significant abundance changes due to genotype were observed for 29.5% of the 6008 compounds (see Experimental Procedures). Remarkably, when considering the 92 (confident and tentatively) annotated compounds, which are mainly hydroxycinnamoyl arabinose derivatives, the abundances of 77 of them (83.7%) were significantly affected by the genotype, indicating that the main impact of *xax1* is on hydroxycinnamoyl arabinose derivatives.

To pinpoint similarly behaving compounds, the regression-fitted mean abundances were subjected to hierarchical cluster analysis (HCA). This yielded six main clusters (Figure 5(c) and Table S2): Cluster A and F were unaffected by genotype and comprise compounds with increasing (cluster A, 2/92 compounds) and decreasing (cluster F, 4/92 compounds) abundance with hydrolysis time. Clusters B, C, D, and E are all genotype-dependent: while cluster E (3/92 compounds) is the only cluster with an increase of abundance in the *xax1* mutant, clusters B (11/92 compounds), C (19/92 compounds), and D (52/92 compounds) all show a reduction of compound abundance compared to WT, with cluster B and C showing additional dependency of compound abundance with hydrolysis time (increased in cluster B and decreased in cluster C). Finally, one of the 92 compounds was affected by genotype, yet did not belong to one of the main clusters (Table S2).

Hydroxycinnamic acid-decorated A xylan side chains are reduced in *xax1*

Consistent with the results from the PACE analysis, abundant compounds detected are hydroxycinnamic acid-modified A: *p*CA-A **8** and **9**, FA-A **12** and **15**, X-(FA)-A-X **10**, X-(FA)-A **13** and **16**, and FA-A-X **18**. All of these compounds are reduced in *xax1*, confirming that hydroxycinnamic acid modifications on arabinosyl substitutions are affected, but importantly, independent of the presence of the additional side chain xylose residue (Figure 5(b)). X-(*p*CA)-A, a structure detected by MALDI-MS, is not among the highly

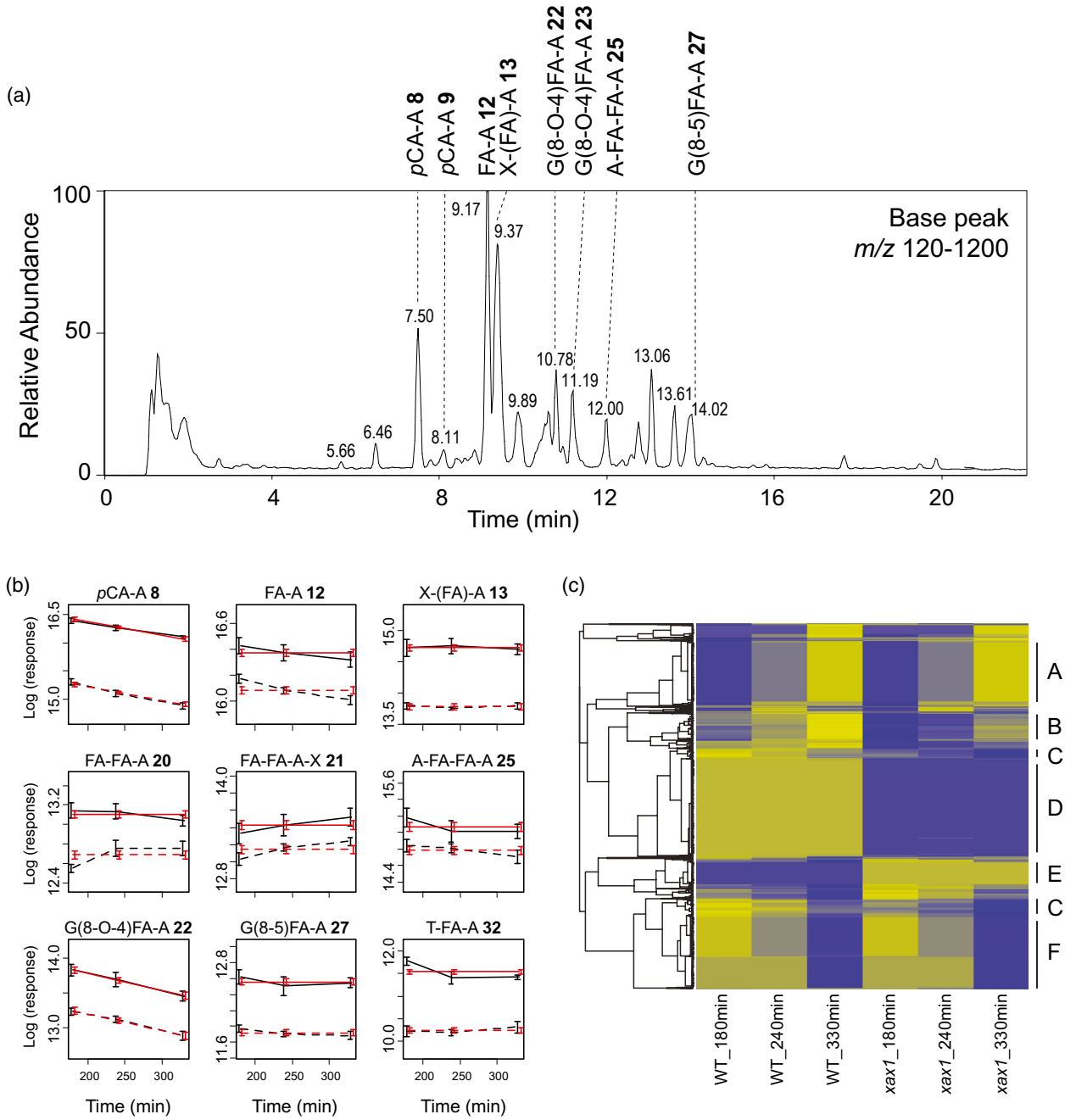

Figure 5. Cell wall phenolic profiling of solid phase-extracted TFA hydrolysates. (a) Base peak chromatogram of WT depicting most abundant structures. (b) Abundance of selected compounds of the phenolic profiling after different hydrolysis times (180, 240, and 330 min) of WT (solid line) and *xax1* (dashed line). Observed means are shown in black, fitted means obtained following piecewise linear regression are shown in red. Error bars, $n = 10$. Note that the retention time is chromatogram-specific rather than the median retention times as shown in Table S2. (c) Heatmap obtained via hierarchical cluster analysis of the fitted means using a distance matrix based on Pearson correlations. Main clusters A–F are indicated on the right side of the heatmap. Color in the heatmap represents the row-based *z*-score varying between −2 (blue) and 2 (yellow).

abundant compounds; however, the LC-MS profiles revealed two isomers with the respective mass (Table S2) and they are also reduced in *xax1*. The MS^2 spectrum recorded for one of them was indicative for the presence of two pentose moieties, supporting an X-(*p*CA)-A or *p*CA-A-X structure with the latter compound containing a xylose from the xylan backbone, which is expected to be sensitive to mild acid hydrolysis. Because a hydrolysis time-dependent change in abundance was observed for only one of the isomers, one isomer is tentatively annotated as *p*CA-A-X and the other as X-(*p*CA)-A. A targeted search also revealed two isomers for each of the X-(*p*CA)-A-X/

Table 1 Differential profiling data of the 32 highly confident, structurally characterized compounds

	Trivial name	Shorthand	Average [log_2(abundance)] WT	Average [log_2(abundance)] *xax*	Average fold change (*xax1*/WT)	HCA cluster
1	Pentose phosphate		12.36	12.36	1.00	F
2	Isocitric acid		12.50	12.95	1.57	E
3	Uridine monophosphate		13.73	13.73	1.00	F
4	Caffeoyl arabinose[a]	CA-A **4**	11.91	11.51	0.67	D
5	3-O-feruloyl quinic acid[a]	FA-Q **5**	10.17	10.48	1.36	E
6	5-O-feruloyl arabinose oxalate ester		11.48	11.22	0.77	C
7	vanilloyl malate		11.81	11.27	0.58	D
8	5-O-*p*-coumaroyl arabinose_1	*p*CA-A **8**	16.26	15.10	0.32	C
9	5-O-*p*-coumaroyl arabinose_2	*p*CA-A **9**	13.58	12.53	0.35	C
10	2′-O-xylopyranosyl-(5′-O-feruloyl)-3-O-arabinofuranosyl xylose	X-(FA)-A-X **10**	13.09	12.55	0.58	C
11	Feruloyl hexuronic acid		12.81	12.54	0.83	D
12	5-O-feruloyl arabinose_1	FA-A **12**	16.37	16.08	0.75	D
13	2-O-xylopyranosyl-(5-O-feruloyl) arabinose_1	X-(FA)-A **13**	14.72	13.77	0.39	D
14	apigenin-6C-hexoside-8C-pentoside[a]		13.65	12.75	0.41	D
15	5-O-feruloyl arabinose_2	FA-A **15**	14.66	14.36	0.81	C
16	2-O-xylopyranosyl-(5-O-feruloyl) arabinose_2	X-(FA)-A **16**	14.52	13.75	0.46	D
17	Ferulic acid	FA **17**	8.53	8.09	0.29	B
18	5′-O-feruloyl-3-O-arabinofuranosyl-xylose	FA-A-X **18**	11.55	10.97	0.56	C
19	ferulic acid	FA **18**	10.53	10.20	0.72	D
20	Ferulic acid homodimer arabinose ester_1	FA-FA-A **20**	13.11	12.69	0.66	D
21	3-O-{5′-O-(ferulic acid homodimer) arabinosyl ester}-xylose	FA-FA-A-X **21**	13.43	13.14	0.76	D
22	guaiacylglycerol-8′′–O–4′-(5-O-feruloyl arabinose) ether_1	G(8–O-4)FA-A **22**	12.56	11.94	0.65	D
23	guaiacylglycerol-8′′–O–4′-(5-O-feruloyl arabinose) ether_2	G(8–O-4)FA-A **23**	14.64	14.15	0.62	D
24	guaiacylglycerol-8′′–O–4′-(5-O-feruloyl arabinose) ether_3	G(8–O-4)FA-A **24**	12.50	12.21	0.75	C
25	5-O-feruloyl arabinose homodimer_1	A-FA-FA-A **25**	15.07	14.79	0.75	D
26	5-O-feruloyl arabinose homodimer_2	A-FA-FA-A **26**	12.89	12.89	1.00	F
27	glycosmisoyl arabinose	G(8–5)FA-A **27**	12.56	11.92	0.53	D
28	Tricin[a]	T **28**	12.89	12.16	0.58	B
29	hydroxyphenylglycerol-8′–O–4-tricin ether	H(8–O-4)T **29**	11.98	11.47	0.60	D
30	guaiacylglycerol-8′–O–4-tricin ether_1	G(8–O-4)T **30**	11.19	10.52	0.52	D
31	guaiacylglycerol-8′–O–4-tricin ether_2	G(8–O-4)T **31**	11.87	11.66	0.81	D
32	tricin-4′′–O–8′/5′-(5-O-feruloyl arabinose) ether	T-FA-A **32**	11.54	10.25	0.28	D

The logarithmically transformed abundance in WT and *xax1* and their fold change values in *xax1*/WT are shown, averaged across the different acid hydrolysis times. Among the listed compounds are isomers, either *Z*/*E* in the case of hydroxycinnamic acid moieties or *threo*/*erythro* in the case of β-aryl ethers (8–O–4-linkages). Compounds classified as hydroxycinnamic acid-modified A are shown in *red*, xylan cross-linking moieties in *green*, and xylan–lignin cross-linking moieties in *blue*.

[a]Compound was detected in extracts obtained from plant material prior to mild acid hydrolysis. See Experimental Procedures and the legend of Table S2 for more details.

*p*CA-A-X-X, in addition to X-(FA)-A-X **10** and two other X-(FA)-A-X/FA-A-X-X isomers (Table S2).

Interestingly, a third hydroxycinnamic acid-modified A, i.e., 5-O-caffeoyl arabinose (CA-A **4**), was detected and also reduced in abundance in *xax1*. The gas phase fragmentation of the anion of CA-A is shown in Figure S2. This finding indicates that A residues, although mainly decorated with FA and *p*CA, can also be decorated with CA. Similar to the FA and *p*CA derivatives, a targeted search revealed one CA-A isomer and X-(CA)-A-X/CA-A-X-X.

Moreover, one abundant compound, also reduced in *xax1*, was elucidated as 5-O-feruloyl arabinose oxalate

ester (FA-A-Ox **6**). The gas phase fragmentation of the anion of FA-A-Ox is shown in Figure S3. Searching for other hydroxycinnamoyl arabinose oxalate esters based on the accurate mass, a putative caffeoyl derivative (CA-A-Ox) was detected, yet no *p*-coumaroyl arabinose oxalate ester could be pinpointed (Table S2). Taken together, we detected a reduction of diverse hydroxycinnamoyl arabinose derivatives, revealing interesting caffeoyl and oxalyl modifications on arabinosyl side chains, all of which were reduced in *xax1*.

Cross-linking of xylan via diferulate linkages to arabinoses is reduced in *xax1*

The phenolic profiling revealed additional highly abundant compounds in WT, which were characterized as radical–radical coupling products between hydroxycinnamic acids and/or hydroxycinnamic acid-modified A (FA-FA-A **20**, FA-FA-A-X **21**, and A-FA-FA-A **25** and **26**; Table 1 and Table S2, Figure 1). A targeted search allowed the detection of many more isomers of radical–radical coupling products between hydroxycinnamic acids and/or hydroxycinnamic acid-modified A (Table S2). In case of diferulates, five and four additional isomers of FA-FA-A **20** and FA-FA-A-X **21**/A-FA-FA-A **25** and **26** could be traced, respectively. In contrast, only two and three putative dicoumarates and dicaffeates were observed, indicating that diferulate linkages are more abundant and more structurally diverse than either dicoumarates or dicaffeates in cross-linking of xylan. Except for A-FA-FA-A **26**, all other ferulate dehydrodimers, i.e., FA-FA-A **20**, FA-FA-A-X **21**, and A-FA-FA-A **25**, were reduced in abundance in *xax1*, suggesting that cross-linking of xylan chains is reduced in the mutant.

Cross-linking of lignin monomers via ferulic acid to arabinose is reduced in *xax1*

Some of the abundant compounds in WT that we could structurally elucidate (Table 1) were radical–radical cross-coupling products between FA-A and the lignin monomer coniferyl alcohol (G(8–O-4)FA-A **22**–**24** and G(8–5)FA-A **27**). A targeted search revealed four additional G-FA-A isomers and seven H-FA-A isomers (i.e., products arising from the coupling of *p*-coumaroyl alcohol with FA-A) that were much less abundant (Table S2). Furthermore, an isomer of G(8–O-4)FA-A-X/X-[G(8–O-4)FA]-A was observed, and two isomers of G(8–O-4)G(8–O-4)FA-A were observed (Table S2). The latter two compounds, representing cross-coupling products of the lignin dimer G(8–O-4)G with FA-A, were too low abundant to obtain clear MS^2 fragmentation data, yet the presence of a pentose moiety could still be inferred from their MS^2 spectra. Similar to FA-A, CA-A seems to enter coupling reactions with coniferyl alcohol as well: A targeted search revealed five G(8–O-4)CA-A, five X[G(8–O-4)CA]-A/G(8–O-4)CA-A-X, and one G(8–O-4)G(8–O-4)CA-A isomer (Table S2). In addition, a radical–radical coupling product of tricin, which is both a flavone and a lignin monomer in monocots (Lan et al., 2015, 2016; del Rio et al., 2012), and feruloyl arabinose (i.e., T-FA-A **32**) was present (Table 1). Tricin explicitly couples via its 4′-O-position (Lan et al., 2015), suggesting that tricin is coupled to FA-A via a 4′-O–5- or 4′-O–8-linkage, hence T-FA-A **32** is likely T(4′-O–5)FA-A or T(4′-O–8)FA-A. A targeted search revealed four additional T-FA-A isomers (Table S2). Cross-coupling products between tricin, coniferyl alcohol, and FA-A seemed also to be present based on the targeted detection of five isomers (Table S2).

The comparison of the WT with *xax1* revealed that clusters C and D, with decreased compound abundance in *xax1*, comprised feruloyl arabinose linked to either coniferyl alcohol or tricin, i.e., G(8–O-4)FA-A **22**, **23**, and **24**, G(8–5)FA-A **27**, and T-FA-A **32**, all of which represent cross-coupling moieties between xylan units and lignin monomers (Table 1). Cluster D also included some lignin dimers, i.e., the dilignols H(8–O-4)T **29** and G(8–O-4)T **30** and **31** (Table S2). These latter two compounds in cluster D suggest that the *xax1* mutation also affects tricin-comprising dilignols.

Taken together, the cell wall-based phenolic profiling revealed a large variety of radical–radical coupled feruloyl arabinose-derived structures, supporting the presence of feruloyl-involved linkages between hemicelluloses and lignin. Most of these structures are reduced in *xax1*, highlighting the complex downstream effects of the *xax1* mutant. The results are consistent with the *xax1* mutation leading to a reduced abundance of hydroxycinnamic acid-modified A side chains on xylan, and this leads to altered xylan cross-linking and reduced xylan coupling to lignin.

DISCUSSION

Chiniquy et al. reported that in the *xax1* mutant of rice, X-A side chains of xylan are absent and the amount of bound hydroxycinnamic acids FA and *p*CA in the plant cell wall is reduced (Chiniquy et al., 2012). Their results suggested that XAX1 is a xylan side chain xylosyltransferase, and that absence of X-A side chains in *xax1* leads to the reduction of cell wall-bound FA and *p*CA observed in *xax1*. Here, we studied the hydroxycinnamic acid-modified xylan side chains and their cross-linking products prepared from *xax1* mutant cell walls. Unexpectedly, the mutation causes a general defect in hydroxycinnamic acid modifications of A side chains of xylan. An alternative and simpler explanation for the *xax1* cell wall phenotype is that XAX1 is a glycosyltransferase that catalyzes the transfer of hydroxycinnamic acid-modified A to the xylan backbone.

The reduction in FA-A, *p*CA-A, and CA-A xylan side chains in *xax1* is hard to explain with the role currently attributed to XAX1 as a β-1,2-xylosyltransferase. If XAX1 were a β-1,2-xylosyltransferase, either an increase or no change in abundance might be expected to occur in hydroxycinnamic acid-modified A side chains lacking the

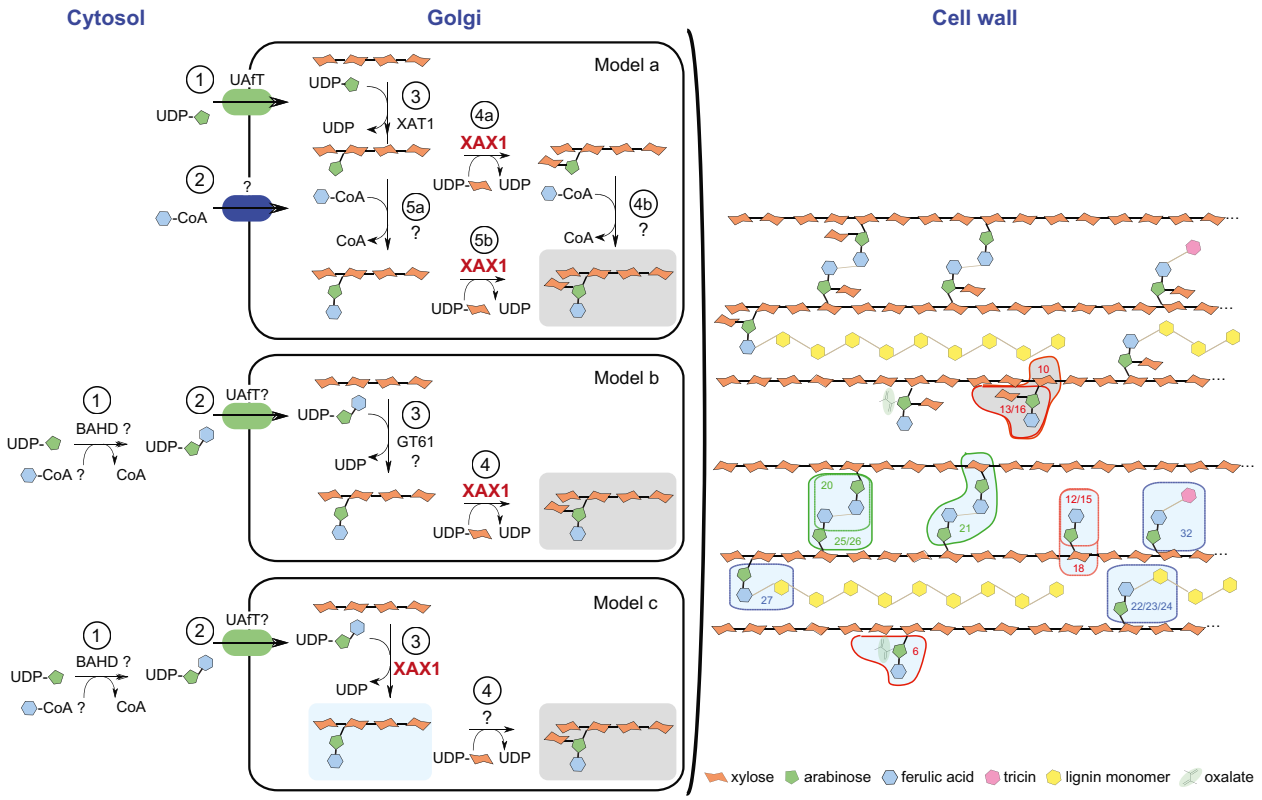

Figure 6. Three models describing putative roles of XAX1 in the biosynthesis of xylan in the Golgi and the resulting potential hydroxycinnamoyl xylan structures in the plant cell wall. On the left, models of the Golgi-localized function of XAX1, where it acts as a β-1,2-xylosyltransferase (models a and b) or as an α-1,3-arabinosyltransferase (model c). The biosynthesis steps are numbered in each model. On the right, structures in the cell wall dependent on XAX1 and modified by any subsequent cross-linking. The hydroxycinnamic acid-modified products depending on XAX1 activity in each model are highlighted, those containing a β-1,2-xylosyl modification in gray, those without in light blue. The compound number is given for those structures that were detected in the LC-MS analysis and shown to be reduced in *xax1* rice cell walls. Note that most compounds reduced in the mutant are blue, consistent with model c. Compounds classified as hydroxycinnamic acid-modified A are shown outlined in *red*, xylan cross-linking moieties in *green*, and xylan–lignin cross-linking moieties in *blue*. For simplicity FA is shown as the hydroxycinnamic acid. Unknown proteins are represented by question marks. UAfT, UDP-Ara*f* Transporter.

β-(1,2)-linked xylose (Figure 6, models a and b). Our results in contrast showed a substantial decrease in abundance of these structures. Unexpectedly, none of the abundant cross-linking structures described in our study possess the xylose branch, even though uncross-linked FA-A and X-(FA)-A may be similarly abundant (Table 1, Figures 4 and 6). This result does not support the proposal that the xylose branch protects the hydroxycinnamic acid substitutions from esterases (Chiniquy et al., 2012). Finally, the quantity of released FA-A and X-(FA)-A was similarly reduced in the *xax1* mutant (Table 1, Figure 4), indicating there is no specific reduction in the xylosylated branches. The proposition of XAX1 acting as a xylosyltransferase was supported by the detection of microsome xylosyltransferase activity upon transient expression in tobacco (*Nicotiana benthamiana*) leaves (Chiniquy et al., 2012). Low activity was detected by measuring incorporation of radioactivity from UDP-[^{14}C]-xylose into an endogenous acceptor. However, the endogenous acceptor in this assay for XAX1 activity is unclear, as 3-linked arabinosyl side chains, the postulated substrate of XAX1, have not been described in dicot leaves.

Apart from XAX1, all so far characterized GT61 Clade A family members have been described to add either 2-linked xylose or 3-linked arabinose to the xylan backbone itself (Anders et al., 2012; Zhong et al., 2018). The more general decrease in arabinose sugars decorated with hydroxycinnamic acids found in the *xax1* mutant therefore could be explained by XAX1 acting as an α-1,3-arabinosyltransferase tolerating hydroxycinnamic acid modifications on an UDP-L-arabinofuranose (UDP-Ara*f*) substrate (Figure 6, model c). The reduction of both xylosylated and non-xylosylated hydroxycinnamoyl arabinose side chains in *xax1* can be explained with this model. Indeed, all the highly abundant cross-linking structures described in our analysis did not contain the xylosyl modification. Moreover, these non-xylosylated hydroxycinnamoyl arabinose cross-linking structures were reduced in *xax1*.

If XAX1 is an α-1,3-arabinosyltransferase, UDP-Ara*f*-FA, UDP-Ara*f*-CA, and UDP-Ara*f*-*p*CA are the potential substrates. These type of sugar donors have not been identified *in planta*, however their presence was suggested based on the finding that several BAHD enzymes (Benzylalcohol O-acetyl transferase, Anthocyanin O-hydroxycinnamoyl transferase, anthranilate N-Hydroxycinnamoyl/benzoyltransferase, Deacetylvindoline 4-O-acetyltransferase) have been described to be involved in the incorporation of hydroxycinnamic acids into xylan (Piston et al., 2010, Bartley et al., 2013, Buanafina et al., 2016, de Souza et al., 2018, de Souza et al., 2019). BAHDs are thought to be cytosolic and therefore the acyl transfer is believed to occur in the cytosol and not in the Golgi lumen (Figure 6; D'Auria, 2006; Mnich et al., 2020). UDP-Ara*f* is synthesized by UDP-arabinopyranose mutase (UAM) in the cytosol as well (Konishi et al., 2007; Rautengarten et al., 2011) and could be ferulated or *p*-coumaroylated by BAHD enzymes and the hydroxycinnamic acid-modified UDP-sugar transferred into the Golgi (Buanafina, 2009; Chateigner-Boutin et al., 2016; Hatfield et al., 2016; Rennie and Scheller, 2014) by an unknown transporter or by the UDP-Araf Transporter (UAfT). Challenging experiments such as *in vitro* enzyme assays and identification of the predicted modified sugar nucleotides are needed to investigate whether XAX1 indeed utilizes UDP-Ara*f*-FA, UDP-Ara*f*-CA, and UDP-Ara*f*-*p*CA substrates to modify xylan.

The fact that hydroxycinnamic acid-modified A and X-A side chains are not completely absent in our analysis of *xax1* suggests redundancy between the GT61s of Clade A enzymes. Extensive phylogenetic analysis of GT61s in monocots revealed that XAX1 belongs to the Poales-specific subgroup GT61-A7, which has only two other members in rice, Os06g27560 and Os01g02910 (Cenci et al., 2018), which could have a similar function to XAX1 in tolerating hydroxycinnamic acid on the UDP-Ara*f* substrate. Interestingly, FA, *p*CA, and CA modifications of xylan appear not equally affected in the *xax1* mutant, which might hint to a preference for specific hydroxycinnamic acid modifications on the donor substrate: *p*CA-A **8** and **9** (0.32- and 0.35-fold change) are much more reduced in *xax1* than either CA-A **4** (0.67-fold change) or FA-A **12** and **15** (0.75- and 0.76-fold change; Table 1). However, in contrast to *p*CA-A, many derivates of FA-A were present. Therefore, when comparing the abundance changes of the FA-A derivate pool with those of *p*CA-A, an unequal effect of the *xax1* mutation on at least the FA and *p*CA modifications of xylan cannot be unambiguously determined.

We did not detect additional more complex structures in the phenolic profiling, such as the α-(1,2)-linked L-galactopyranosyl sugar of X-(FA)-A, which have been previously detected in leaf tissues from several grasses (Wende and Fry, 1997). This might be due to their lower abundance or due to their reduced hydrophobicity, leading to weaker interactions with the C18 stationary phase. However, the detection of minor amounts of galactose in the monosaccharide analysis of the SPE eluent fractions (Table S1) might suggest the presence of such structures. However, we detected a structure, which most likely shows an Ox modification of the A side chain of xylan in the plant cell wall. Ox modifications were suggested to exist in the plant cell wall based on polysaccharide acyltransferase activity detected *in vitro* (Dewhirst and Fry, 2018).

The changes in xylan side chain biosynthesis facilitated by XAX1 result in enhanced saccharification and extraction of xylan in *xax1* hinting to altered interactions of xylan in the plant cell wall, while the cellulose content and the size of xylan molecules remained unchanged (Chiniquy et al., 2012). Our study shows that enhanced saccharification is due to lowered cross-linking through FA as summarized in Figure 6. Except for A-FA-FA-A **26**, all diferulates detected and all molecules derived from a lignin monomer coniferyl alcohol cross-coupled to 5-O-feruloyl arabinose (G-FA-A) were less abundant in *xax1*. In addition, dicoumarates, dicaffeates, and all putative G-CA-A structures were reduced in *xax1* (Table S2).

Xylans are linked via radical–radical cross-coupling of the ferulate moieties present on the xylan A side chains to lignin and other xylan chains. The cross-coupling versatility is illustrated by the detection of a wide variety of diferulate isomers, i.e., 8–O-4′, 8–8′, 8–5′, 5–5′, and 5–O-4′, with the 5–5′-linkage being the most frequent (Bento-Silva et al., 2018; Ralph, 2010; Ralph et al., 2004; Waterstraat and Bunzel, 2018). Our findings further substantiated this through the detection of (i) different linkages, i.e., 8–O-4′ and 8–5′, in the G-FA-A cross-coupling products, (ii) lignin units other than G units (H units) attached to FA-A, (iii) cross-coupling products between ferulates and minor lignin monomers such as tricin, i.e., T-FA-A **32**, and (iv) detection of dicaffeates and several G-CA-A isomers, representing dicaffeates as potential novel lignin–xylan bridging structures. CA is abundant in plants as an intermediate of lignin biosynthesis; to our knowledge it has not been described to modify xylan in rice, but it was identified in LC-MS analysis as one of the phenolic acid compounds bound to xylan in Kodo millet (Bijalwan et al., 2016).

In studies with synthetic lignins and monocot lignins (Ralph, 2010; Ralph et al., 1995, 2019), monolignols preferentially couple with their 8-position to ferulate esters yielding mainly G(8–O-4)FA, G(8–5)FA, and G(8–8)FA moieties. The strong prevalence of the 8–O-4-linkages in the here characterized G-FA-A cross-coupled structures are consistent with the 'end-wise' polymerization process of lignification, which postulates that monolignols slowly diffusing into the lignification zone will preferentially couple with an existing polymer rather than with another monomer (Ralph

et al., 2004). As the hemicellulose network is laid down before lignification starts, the first monolignols that enter the cell wall will likely couple with the FA-A moieties that are linked to the hemicellulose network (Grabber et al., 2002). Most of these cross-couplings lead to the formation of the coniferyl alcohol coupled via its 8-position to the phenol function (4-O position; the two most abundant peaks associated with G-FA-A products in Figure 5(a) are G (8–O-4)FA-A isomers) of the FA-A moiety, rendering FA unavailable for further oxidation. Further cross-linking of the G(8–O-4)FA-A structure can only occur via oxidation of the phenol function present on the coniferyl alcohol-derived, i.e., guaiacyl, unit. In case of an incoming coniferyl alcohol molecule, this would yield G(8–O-4)G(8–O-4)FA-A. Interestingly, our analysis indeed detected putative bridging structures between lignin and xylan of higher molecular weight, i.e., G(8–O-4)G(8–O-4)FA-A and X-[G(8–O-4)FA]-A/G(8–O-4)FA-A-X, supporting the idea of 'end-wise' polymerization to occur *in vivo*. Apart from laccases and peroxidases, which have been characterized as key factors in the spatio-temporal regulation of lignin polymerization (Tobimatsu and Schuetz, 2019), the xylan structure with the presence or absence of FA-A, *p*CA-A, or CA-A side chains will direct lignification as well, the latter possibly regulated by the activity of XAX1 and its homologs.

Our data show that the GT61 XAX1 is a key player in the synthesis of xylan hydroxycinnamoyl arabinose moieties. We therefore propose an alternative role for the XAX1 glycosyltransferase in that it directly transfers FA-A, *p*CA-A, and, interestingly, also CA-A side chains to xylan. As a result of this activity, the levels of various hydroxycinnamate–hydroxycinnamate and monolignol–hydroxycinnamate coupling products are depleted in *xax1*. Furthermore, the characterized coupling products between lignin, FA, and A suggest that XAX1-dependent FA-A moieties on xylan initiate lignin polymerization. All of this emphasizes the importance of XAX1 in establishing both xylan–xylan and lignin–xylan cross-links.

EXPERIMENTAL PROCEDURES

Plant material and growth conditions

The rice GT61 (*O. sativa* L. ssp. *japonica*) transfer DNA (T-DNA) insertion mutant seeds for *XAX1* were generously provided by Dr. Pamela Ronald and Dr. Henrik Scheller (Lawrence Berkeley National laboratory, US). Rice GT61 T-DNA insertion mutants were genotyped using the primer sequences described in (Chiniquy et al., 2012). Segregating WT was used as control in all experiments.

Rice dehulled seeds were surface-sterilized by shaking in a 3% bleach solution at 1200 rpm for 10 min. Seeds were rinsed four times with autoclaved milliQ water. The seeds were germinated at 30°C on a humidified filter paper and then transferred to Silica Sand. Once the plants reached the tillering developmental stage, they were transferred to a 1:1 Silica Sand/soil mixture. Plants were grown at 28°C (day)/23°C (night), 60% humidity, 60% ambient CO_2, and 12 h light (400 μmol/m^2) and kept under constant watering conditions, supplemented weekly with a 500× diluted Poliverdol® solution and 0.1 g L^{-1} of Sequestrene Rapid®.

Alcohol-insoluble residue preparation

Tissue of mature rice leaves was harvested in 96% ethanol and incubated in a water bath at 70°C for 30 min. After cooling down, the tissues were ball-milled using a mixer mill MM400 at 20 rotations per second, three times for 5 min each. The homogenized tissue was centrifuged and the pellet was subjected to several washes to remove proteins, lipids, and other non-polysaccharide components. This procedure included washing the pellet with 100% ethanol, followed by overnight treatment with 2:3 (v/v) of methanol: chloroform and a sequential set of washes with 100, 65, 80, and 100% ethanol. The pellet obtained after these washes corresponded to the AIR, which was dried and stored at room temperature.

Mild acid hydrolysis

Mild acid hydrolysis was performed on AIR samples using 50 mM TFA, taking the appropriate measures to prevent TFA evaporation. This procedure was carried out at 100°C in a heat block, for different time intervals, as indicated in the respective experiments. A TFA hydrolysis time of 240 min was chosen for the analysis by MALDI-MS in order to reach maximal release of the hydroxycinnamic acid-modified structures. Samples were cooled down on ice and centrifuged and the supernatant was collected. The pellet was washed and the supernatant was pooled with the supernatant collected previously. Supernatant samples were dried in a vacuum concentrator overnight at room temperature.

Solid phase extraction with C18 Cartridges

Sep-Pak C18 Classic Cartridges were washed with 100% ethanol, milliQ water, and 100% acetonitrile to remove potential contaminants (Ishii, 1991). The cartridge was then equilibrated with 20 mM ammonium acetate buffer (adjusted to pH 7 with acetic acid). Lyophilized samples obtained from mild TFA hydrolysis were resuspended in 20 mM ammonium acetate buffer (pH 7) and loaded on the cartridge. The C18 Cartridges were washed with milliQ water and 10% ethanol and the sample was eluted with 5 ml of increasing percentages of ethanol of 15, 18, and 20%. Four fractions were collected for each ethanol elution. Full elution of the bound oligosaccharides was achieved with a single 100% ethanol wash. Fractions were dried in a vacuum concentrator at 55°C.

Enzyme hydrolysis

Solid phase extracts were hydrolyzed using xylosidase GH3 from *C. globosum* (Tryfona et al., 2019), a generous gift from Novozymes (*Cg*GH3, NS39127). Enzyme was added at a final concentration of 2 μM and digestions were carried out overnight at room temperature in 0.1 M ammonium acetate buffer (pH 5.5) under constant shaking. Enzymes were inactivated at 100°C for 10 min and the sample was dried in a vacuum concentrator at 45°C.

Alkali treatment

Solid phase extracts were alkali-treated with 4 M NaOH for 1 h at room temperature to cleave ester linkages. Samples were subsequently neutralized to pH 7 with 1 M HCl and the samples were dried in a vacuum concentrator at 45°C.

Monosaccharide analysis

Monosaccharide analysis was performed by subjecting three biological replicates of AIR to 2 M TFA hydrolysis at 120°C for 1 h.

After SPE and washing the cartridges with milliQ water and 10% ethanol, the samples were eluted with 100% ethanol. Monosaccharide detection was performed by high-performance anion exchange chromatography with pulsed amperometric detection (HPAEC-PAD) as described in (Tryfona et al., 2012).

Polysaccharide analysis by carbohydrate gel electrophoresis

Samples and xylooligosaccharide standard X_1–X_6 were derivatized by reductive amination with 8-aminonaphthalene-1,3,6-trisulfonic acid (ANTS). The derivatization reaction was carried out with a mix containing 5 μl of ANTS, 5 μl of 0.2 M of 2-picoline-borane (2-PB), and 10 μl of a freshly prepared buffer containing 30 μl of acetic acid, 170 μl of milliQ water, and 200 μl of DMSO. Derivatization was carried out at 37°C overnight. Derivatized samples were lyophilized in a vacuum concentrator at 60°C and resuspended in 100 μl of 3 M urea to solubilize the labeled oligosaccharides. Samples were loaded on polyacrylamide gels and electrophoresed at 10°C at 200 V for 30 min, followed by 1000 V for 1 h and 40 min. A 0.1 M TRIS-borate (pH 8.2) solution was used as the running buffer. Labeled products on the PACE gel were detected using a G-Box CCD camera with a transilluminator with long-wave tubes emitting at 365 nm. Images were captured using GeneSnap software.

Quantification was carried out on three biological replicates of WT and *xax1* leaf AIR using Genetools software. Aliquots of 20, 40, and 100 picomol of a mix containing ANTS-labeled xylose, xylobiose, and xylotriose were loaded on the gel. These standards were used to build a calibration curve in Genetools. This procedure allowed the software to determine the mol quantities of the oligosaccharides in PACE bands by linear regression. Significance of the differences detected was assessed at the 5% level using Student's *t*-test.

Mass spectrometry

SPE was carried out on mild acid hydrolysates as described above, with a C18 SPE Cartridge with 1 g of packing to allow for the purification of higher amounts of sample. Eluted ethanol fractions were dried in a vacuum concentrator at room temperature. Samples were resuspended in water and manually spotted on a MALDI plate with procainamide hydrochloride as described previously (Lavanant and Loutelier-Bourhis, 2012). Procainamide hydrochloride was used as a derivatizing co-matrix to add mass to the products of the C18 fractions, which are expected to be considerably small and could have their masses obscured by matrix peaks in the MALDI spectrum. After air-drying, the sample spots were overlaid with 1 μl 2,5-DHB matrix (10 mg ml^{-1} in 50% aqueous methanol) and analyzed by MALDI-ToF/ToF–MS on an AB-Sciex 4700. The MS spectra were acquired with an average of 10 000 laser shots per spectrum in positive ion mode (mass range 250–1500 Da). The observed ions are protonated.

Liquid chromatography–mass spectrometry

Mild acid hydrolysis (50 mM TFA, 100°C) was performed on AIR samples from mature leaves of five biological replicates of WT and *xax1* and for two technical replicates of each biological replicate. Three time points of mild acid hydrolysis (180, 240, and 330 min) were analyzed for each sample. The lyophilized samples were dissolved in 200 μl milliQ water, of which 10 μl was profiled by a reverse phase (Acquity UHPLC BEH C18 column, 2.1 × 150 mm, 1.7 μm; column temperature 80°C) Accela UHPLC system coupled to FTICR-MS (LTQ FT Ultra) via electrospray ionization (ESI) operated in negative ionization mode (spray voltage −3.5 kV, sheath gas 30 [arb], aux gas 10 [arb], capillary temperature 300°C). Other instrumental conditions were as previously described with minor modifications (Morreel et al., 2014). LC solvents were acidified with 0.1% formic acid. A reversed phase gradient was applied in which the proportion of acetonitrile increased from 1% (0 min) to 50% (30 min). LC-MS feature integration, feature grouping, and chromatogram alignment methods have been described previously (Morreel et al., 2014). In total, 41 542 *m/z* features were integrated that were further grouped into 6008 *m/z* feature groups. This is necessary as each compound is represented by multiple *m/z* features; hence, the number of *m/z* feature groups is an estimation of the number of profiled compounds. However, for many *m/z* feature groups, not all *m/z* features belonging to the same compound were included based on visual inspection of the chromatograms. Therefore, the number of *m/z* feature groups still represents an overestimation of the real number of profiled compounds. Nevertheless, the low number of data points across the peak of an *m/z* feature in an FT full MS spectrum hinders a more efficient deconvolution. Statistical analyses were performed on the most abundant *m/z* feature in each group, as this was the pseudo-molecular ion in most cases. The phenolic profiling results are described in terms of compounds rather than *m/z* feature groups.

MS-based structural elucidation

Structural elucidation of the negative ion MS^n data was based on the accurately recorded *m/z* value of the compound (using either the base peak or the ^{13}C isotope peak dependent on which one served as precursor ion for MS^n recording; see Table S2), previously published MS^n data of phenylpropanoids, (neo)lignans and oligolignols (Morreel et al., 2014), and 5-O-feruloyl-L-arabinose (Quemener and Ralet, 2004), and knowledge of MS-based sugar cross-ring cleavages for various di- and oligosaccharides (Carroll et al., 1995; Dallinga and Heerma, 1991; March and Stadey, 2005; Mulroney et al., 1999; Quemener et al., 2006). A more in-depth description of the effect of the glycosidic bond on the cross-ring cleavages is given as Methods S1. Whenever possible, the aglycone moiety was verified via spectral matching to the MS^n spectra of a standard compound. This set of structurally characterized compounds was then used to trace other isomers or structurally similar compounds in which the aglycone moiety was represented by another phenylpropanoid/monolignol using the R-based RDynLib package (Desmet et al., 2021). For the latter approach, the presence of the putative compound was only based on the chemical formula that was computed from the accurately recorded *m/z* value.

LC-MS data mining

R version 3.2.3 (R Core Team, 2013) was used for all statistical analyses. For each *m/z* feature group, changes in the abundance of the selected *m/z* feature were modeled via piecewise linear regression (lm function). Missing data were replaced by an arbitrarily chosen threshold value (100). Technical replicates were averaged before modeling and all data were logarithmically (natural logarithm) transformed. Starting from a full model including the mild acid hydrolysis time, genotype, and the appropriate interaction terms, those terms showing the least significant Wald test *P*-value ($P_{term} > 0.05$) and those that were not included in any higher-order interaction terms were iteratively removed. Model comparison was performed using the anova() function. Based on a $P_{model} < 0.001$ criterion, 2480 *m/z* feature groups (i.e., 100×2480/

6008 = 41.3% of the feature groups) showed a significantly changed abundance between samples that differed in the applied hydrolysis time and/or genotype. However, for two of these 2480 *m/z* feature groups, none of the model terms was significant. Of the remaining 2478 *m/z* feature groups, the abundances of 494 (8.2%), 707 (11.8%), and 1093 (18.2%) *m/z* features were due to the effect of the genotype ($P_{genotype} < 0.05$), the hydrolysis time ($P_{time} < 0.05$), and both the genotype and the hydrolysis time ($P_{genotype} < 0.05$ and $P_{time} < 0.05$). The abundances of only 184 (3.1%) *m/z* features were governed by a genotype × hydrolysis time interaction effect ($P_{genotype \times time} < 0.05$ and/or $P_{genotype \times knot} < 0.05$). Thus, 29.5% (8.2% + 18.2% + 3.1%) and 33.1% (11.8% + 18.2% + 3.1%) of the *m/z* feature groups were affected by genotype and hydrolysis time, respectively.

HCA (hclust() function) was performed on the regression-derived fitted mean abundances for the presumed pseudo-molecular ion from each of the *m/z* feature groups using the Pearson correlation matrix as distance matrix; a heatmap was returned with the heatmap.2() function (gplots package). HCA yielded six main clusters (A–F). HCA clustering results were much improved by including the regression-fitted mean values rather than the raw data-based mean abundances. Nevertheless, sometimes isomeric compounds were classified into two different HCA clusters because the curvature in the raw data-based feature abundance profile of only one of them reached the significance threshold during regression modeling and, hence, was retained in the model. For example, FA-A **12** and FA-A **15** are likely the *Z* and *E* isomers of 5-O-feruloyl arabinose, which are mutually converted due to UV light. Thus, although their abundances should be correlated, they are members of different HCA clusters, i.e., clusters D and C. Cluster D is comprised of compounds that have horizontal abundance profiles across the various TFA hydrolysis times but are higher in WT than in *xax1*. Cluster C is comprised of compounds that have abundances that decrease with hydrolysis time but are on average higher in WT than in *xax1*. The cluster D classification of FA-A **12** is evident from the red regression profile for this compound in Figure 5(b). However, the feature abundance profile of the raw data shows a decreasing trend with increasing hydrolysis time. Clearly, this decrease was not significant enough to classify FA-A **12** as a cluster C member.

ACKNOWLEDGMENTS

The authors are grateful for the funding sources that allowed this work to be carried out: CF was funded by the BBSRC Doctoral Training Programme (BB/J014540/1); NA was funded by the Cambridge BBSRC (BB/K005537/1). We also acknowledge the Bijzonder Onderzoeksfonds-Zware Apparatuur of Ghent University for use of the FTICR-MS (174PZA05). The authors would also like to acknowledge the technical support provided by Rita Marques and Xiaolan Yu and thank Lucio Mendonça, who helped develop the protocol for feruloyl oligosaccharide purification and characterization. We also thank Henrik Scheller and Pamela Ronald for plant material provided and Novozymes for glycoside hydrolase enzymes.

AUTHOR CONTRIBUTION

Conceptualization, CF, NA, and PD; methodology, CF, KM, TT, TK, MB-W, WB, and PD; formal analysis, CF, KM, TT, and NA; investigation, CF, KM, and TT; writing – original draft preparation, CF, KM, and NA; writing – review & editing, KM, NA, WB, and PD; visualization, CF, KM, TT, and NA; supervision, NA, WB, and PD; funding acquisition, CF, KM, WB, and PD.

CONFLICT OF INTEREST

The authors declare no conflict of interest.

DATA AVAILABILITY STATEMENT

All relevant data can be found within the manuscript and its supporting materials. To obtain raw data or materials, please contact the corresponding authors.

SUPPORTING INFORMATION

Additional Supporting Information may be found in the online version of this article.

Figure S1. PACE analysis of NaOH-sensitive xylan hydrolysis products in SPE eluates.

Figure S2. Gas phase fragmentation of the anion of caffeoyl arabinose (CA-A **4**).

Figure S3. Gas phase fragmentation of the anion of 5-O-feruloyl arabinose oxalate ester (FA-A-Ox **6**).

Table S1. Monosaccharide composition of WT AIR.

Table S2. Structural assignment of compounds and statistical data.

REFERENCES

Abramson, M., Shoseyov, O. & Shani, Z. (2010) Plant cell wall reconstruction toward improved lignocellulosic production and processability. *Plant Science*, **178**, 61–72.

Allerdings, E., Ralph, J., Steinhart, H. & Bunzel, M. (2006) Isolation and structural identification of complex feruloylated heteroxylan side-chains from maize bran. *Phytochemistry*, **67**, 1276–1286.

Anders, N., Wilkinson, M.D., Lovegrove, A., Freeman, J., Tryfona, T., Pellny, T.K. *et al.* (2012) Glycosyl transferases in family 61 mediate arabinofuranosyl transfer onto xylan in grasses. *Proceedings of the National Academy of Sciences*, **109**, 989–993.

Bartley, L.E., Peck, M.L., Kim, S.R., Ebert, B., Manisseri, C., Chiniquy, D.M. *et al.* (2013) Overexpression of a BAHD acyltransferase, OsAt10, alters rice cell wall hydroxycinnamic acid content and saccharification. *Plant Physiology*, **161**, 1615–1633.

Bencur, P., Steinkellner, H., Svoboda, B., Mucha, J., Strasser, R., Kolarich, D. *et al.* (2005) Arabidopsis thaliana beta1,2-xylosyltransferase: an unusual glycosyltransferase with the potential to act at multiple stages of the plant N-glycosylation pathway. *The Biochemical Journal*, **388**, 515–525.

Bento-Silva, A., Patto, M.C.V. & Bronze, M.D. (2018) Relevance, structure and analysis of ferulic acid in maize cell walls. *Food Chemistry*, **246**, 360–378.

Bhatia, R., Gallagher, J.A., Gomez, L.D. & Bosch, M. (2017) Genetic engineering of grass cell wall polysaccharides for biorefining. *Plant Biotechnology Journal*, **15**, 1071–1092.

Bijalwan, V., Ali, U., Kesarwani, A.K., Yadav, K. and Mazumder, K. (2016) Hydroxycinnamic acid bound arabinoxylans from millet brans-structural features and antioxidant activity. *International Journal of Biological Macromolecules*, **88**, 296–305.

Bowman, M.J., Dien, B.S., O'Bryan, P.J., Sarath, G. & Cotta, M.A. (2011) Selective chemical oxidation and depolymerization of switchgrass (Panicum virgatum L.) xylan with oligosaccharide product analysis by mass spectrometry (vol 25, pg 941, 2011). *Rapid Commun Mass Sp*, **25**, 1686.

Buanafina, M.M.D. (2009) Feruloylation in grasses: current and future perspectives. *Molecular Plant*, **2**, 861–872.

Buanafina, M.M., Fescemyer, H.W., Sharma, M. & Shearer, E.A. (2016) Functional testing of a PF02458 homologue of putative rice arabinoxylan feruloyl transferase genes in Brachypodium distachyon. *Planta*, **243**, 659–674.

Bunzel, M., Ralph, J., Lu, F., Hatfield, R.D. & Steinhart, H. (2004) Lignins and ferulate-coniferyl alcohol cross-coupling products in cereal grains. *Journal of Agriculture and Food Chemistry*, **52**, 6496–6502.

Burr, S.J. & Fry, S.C. (2009) Extracellular cross-linking of maize arabinoxylans by oxidation of feruloyl esters to form oligoferuloyl esters and ether-like bonds. *The Plant Journal*, **58**, 554–567.

Busse-Wicher, M., Gomes, T.C., Tryfona, T., Nikolovski, N., Stott, K., Grantham, N.J. *et al.* (2014) The pattern of xylan acetylation suggests xylan may interact with cellulose microfibrils as a twofold helical screw in the secondary plant cell wall of Arabidopsis thaliana. *The Plant Journal*, **79**, 492–506.

Carroll, J.A., Willard, D. & Lebrilla, C.B. (1995) Energetics of cross-ring cleavages and their relevance to the linkage determination of oligosaccharides. *Analytica Chimica Acta*, **307**, 431–447.

Cenci, A., Chantret, N. & Rouard, M. (2018) Glycosyltransferase family 61 in liliopsida (Monocot): the story of a gene family expansion. *Frontiers in Plant Science*, **9**.

Chateigner-Boutin, A.L., Ordaz-Ortiz, J.J., Alvarado, C., Bouchet, B., Durand, S., Verhertbruggen, Y. *et al.* (2016) Developing pericarp of maize: a model to study arabinoxylan synthesis and feruloylation. *Frontiers in Plant Science*, **7**, 1476.

Chiniquy, D., Sharma, V., Schultink, A., Baidoo, E.E., Rautengarten, C., Cheng, K. *et al.* (2012) XAX1 from glycosyltransferase family 61 mediates xylosyltransfer to rice xylan. *Proceedings of the National Academy of Sciences*, **109**, 17117–17122.

Dallinga, J.W. & Heerma, W. (1991) Reaction mechanism and fragment ion structure determination of deprotonated small oligosaccharides, studied by negative ion fast atom bombardment (tandem) mass spectrometry. *Biological Mass Spectrometry*, **20**, 215–231.

D'Auria, J.C. (2006) Acyltransferases in plants: a good time to be BAHD. *Current Opinion in Plant Biology*, **9**, 331–340.

de Oliveira, D.M., Finger-Teixeira, A., Mota, T.R., Salvador, V.H., Moreira-Vilar, F.C., Molinari, H.B.C. *et al.* (2015) Ferulic acid: a key component in grass lignocellulose recalcitrance to hydrolysis. *Plant Biotechnology Journal*, **13**, 1224–1232.

de Souza, W.R., Martins, P.K., Freeman, J., Pellny, T.K., Michaelson, L.V., Sampaio, B.L. *et al.* (2018) Suppression of a single BAHD gene in Setaria viridis causes large, stable decreases in cell wall feruloylation and increases biomass digestibility. *New Phytologist*, **218**, 81–93.

de Souza, W.R., Pacheco, T.F., Duarte, K.E., Sampaio, B.L., de Oliveira Molinari, P.A., Martins, P.K. *et al.* (2019) Silencing of a BAHD acyltransferase in sugarcane increases biomass digestibility. *Biotechnology for Biofuels*, **12**, 111.

del Rio, J.C., Rencoret, J., Prinsen, P., Martinez, A.T., Ralph, J. & Gutierrez, A. (2012) Structural characterization of wheat straw lignin as revealed by analytical pyrolysis, 2D-NMR, and reductive cleavage methods. *Journal of Agricultural and Food Chemistry*, **60**, 5922–5935.

Desmet, S., Saeys, Y., Verstaen, K., Dauwe, R., Kim, H., Niculaes, C. *et al.* (2021) Maize specialized metabolome networks reveal organ-preferential mixed glycosides. *Computational and Structural Biotechnology Journal*, **19**, 1127–1144.

Dewhirst, R.A. & Fry, S.C. (2018) Oxalyltransferase, a plant cell-wall acyltransferase activity, transfers oxalate groups from ascorbate metabolites to carbohydrates. *Plant Journal*, **95**, 743–757.

Ebringerova, A., Hromadkova, Z. & Heinze, T. (2005) Hemicellulose. *Polysaccharides 1: Structure. Characterization and Use*, **186**, 1–67.

Ford, C.W. & Hartley, R.D. (1989) Gc/Ms Characterization of Cyclodimers from Para-Coumaric and Ferulic Acids by Photodimerization - a Possible Factor Influencing Cell-Wall Biodegradability. *Journal of the Science of Food and Agriculture*, **46**, 301–310.

Ford, C.W. & Hartley, R.D. (1990) Cyclodimers of P-coumaric and ferulic acids in the cell-walls of tropical grasses. *Journal of the Science of Food and Agriculture*, **50**, 29–43.

Freeman, J., Ward, J.L., Kosik, O., Lovegrove, A., Wilkinson, M.D., Shewry, P.R. *et al.* (2017) Feruloylation and structure of arabinoxylan in wheat endosperm cell walls from RNAi lines with suppression of genes responsible for backbone synthesis and decoration. *Plant Biotechnology Journal*, **15**, 1429–1438.

Freudenberg, K. & Neish, A.C. (1968) *Constitution and biosynthesis of lignin*. Berlin: Springer-Verlag.

Gao, Y.P., He, C.W., Zhang, D.M., Liu, X.L., Xu, Z.P., Tian, Y.B. *et al.* (2017) Two trichome birefringence-like proteins mediate xylan acetylation, which is essential for leaf blight resistance in rice. *Plant Physiology*, **173**, 470–481.

Grabber, J.H., Hatfield, R.D., Ralph, J., Zon, J. & Amrhein, N. (1995) Ferulate cross-linking in cell-walls isolated from maize cell-suspensions. *Phytochemistry*, **40**, 1077–1082.

Grabber, J.H., Ralph, J. & Hatfield, R.D. (2000) Cross-linking of maize walls by ferulate dimerization and incorporation into lignin. *Journal of Agriculture and Food Chemistry*, **48**, 6106–6113.

Grabber, J.H., Ralph, J. & Hatfield, R.D. (2002) Model studies of ferulate-coniferyl alcohol cross-product formation in primary maize walls: implications for lignification in grasses. *Journal of Agriculture and Food Chemistry*, **50**, 6008–6016.

Hatfield, R.D., Rancour, D.M. & Marita, J.M. (2016) Grass cell walls: a story of cross-linking. *Frontiers in Plant Science*, **7**, 2056.

Ishii, T. (1991) Isolation and characterization of a diferuloyl arabinoxylan hexasaccharide from bamboo shoot cell-walls. *Carbohydrate Research*, **219**, 15–22.

Ishii, T. (1997) Structure and functions of feruloylated polysaccharides. *Plant Science*, **127**, 111–127.

Jacquet, G., Pollet, B., Lapierre, C., Mhamdi, F. & Rolando, C. (1995) New ether-linked ferulic acid-coniferyl alcohol dimers identified in grass straws. *Journal of Agricultural and Food Chemistry*, **43**, 2746–2751.

Konishi, T., Takeda, T., Miyazaki, Y., Ohnishi-Kameyama, M., Hayashi, T., O'Neill, M.A. *et al.* (2007) A plant mutase that interconverts UDP-arabinofuranose and UDP-arabinopyranose. *Glycobiology*, **17**, 345–354.

Lan, W., Lu, F.C., Regner, M., Zhu, Y.M., Rencoret, J., Ralph, S.A. *et al.* (2015) Tricin, a flavonoid monomer in monocot lignification. *Plant Physiology*, **167**, 1284–U1265.

Lan, W., Morreel, K., Lu, F.C., Rencoret, J., del Rio, J.C., Voorend, W. *et al.* (2016) Maize tricin-oligolignol metabolites and their implications for monocot lignification. *Plant Physiology*, **171**, 810–820.

Lapierre, C., Voxeur, A., Boutet, S. & Ralph, J. (2019) Arabinose conjugates diagnostic of ferulate-ferulate and ferulate-monolignol cross-coupling are released by mild acidolysis of grass cell walls. *Journal of Agriculture and Food Chemistry*, **67**, 12962–12971.

Lavanant, H. & Loutelier-Bourhis, C. (2012) Use of procaine and procainamide as derivatizing co-matrices for the analysis of oligosaccharides by matrix-assisted laser desorption/ionization time-of-flight mass spectrometry. *Rapid Communications in Mass Spectrometry*, **26**, 1311–1319.

Lerouxel, O., Choo, T.S., Seveno, M., Usadel, B., Faye, L., Lerouge, P. *et al.* (2002) Rapid structural phenotyping of plant cell wall mutants by enzymatic oligosaccharide fingerprinting. *Plant Physiology*, **130**, 1754–1763.

March, R.E. & Stadey, C.J. (2005) A tandem mass spectrometric study of saccharides at high mass resolution. *Rapid Communications in Mass Spectrometry*, **19**, 805–812.

Mnich, E., Bjarnholt, N., Eudes, A., Harholt, J., Holland, C., Jorgensen, B. *et al.* (2020) Phenolic cross-links: building and de-constructing the plant cell wall. *Natural Products Reports*, **37**, 919–961.

Morreel, K., Saeys, Y., Dima, O., Lu, F.C., Van de Peer, Y., Vanholme, R. *et al.* (2014) Systematic structural characterization of metabolites in Arabidopsis via candidate substrate-product pair networks. *The Plant Cell*, **26**, 929–945.

Mulroney, B., Barrie Peel, J. & Traeger, J.C. (1999) Theoretical study of deprotonated glucopyranosyl disaccharide fragmentation. *Journal of Mass Spectrometry*, **34**, 856–871.

Pauly, M. & Keegstra, K. (2008) Cell-wall carbohydrates and their modification as a resource for biofuels. *Plant Journal*, **54**, 559–568.

Piston, F., Uauy, C., Fu, L., Langston, J., Labavitch, J. & Dubcovsky, J. (2010) Down-regulation of four putative arabinoxylan feruloyl transferase genes from family PF02458 reduces ester-linked ferulate content in rice cell walls. *Planta*, **231**, 677–691.

Quemener, B., Ordaz-Ortiz, J.J. & Saulnier, L. (2006) Structural characterization of underivatized arabino-xylo-oligosaccharides by negative-ion electrospray mass spectrometry. *Carbohydrate Research*, **341**, 1834–1847.

Quemener, B. & Ralet, M.C. (2004) Evidence for linkage position determination in known feruloylated mono- and disaccharides using electrospray ion trap mass spectrometry. *Journal of Mass Spectrometry*, **39**, 1153–1160.

Quideau, S. & Ralph, J. (1997) Lignin-ferulate cross-links in grasses.4. Incorporation of 5-5-coupled dehydrodiferulate into synthetic lignin. *Journal of the Chemical Society, Perkin Transactions 1*, **1**, 2351–2358.

Ralph, J. (2010) Hydroxycinnamates in Lignification. *Phytochemistry Reviews*, **9**, 65–83.

Ralph, J., Bunzel, M., Marita, J.M., Hatfield, R.D., Lu, F., Kim, H. *et al.* (2004) Peroxidase-dependent cross-linking reactions of p-hydroxycinnamates in plant cell walls. *Phytochemistry Reviews*, **3**, 79–96.

Ralph, J., Grabber, J.H. & Hatfield, R.D. (1995) Lignin-Ferulate Cross-Links in Grasses - Active Incorporation of Ferulate Polysaccharide Esters into Ryegrass Lignins. *Carbohydrate Research*, **275**, 167–178.

Ralph, J., Helm, R.F., Quideau, S. & Hatfield, R.D. (1992) Lignin Feruloyl Ester Cross-Links in Grasses. 1. Incorporation of Feruloyl Esters into Coniferyl Alcohol Dehydrogenation Polymers. *Journal of the Chemical Society, Perkin Transactions* **1**, 2961–2969.

Ralph, J., Lapierre, C. & Boerjan, W. (2019) Lignin structure and its engineering. *Curr Opin Biotech*, **56**, 240–249.

Rautengarten, C., Ebert, B., Herter, T., Petzold, C.J., Ishii, T., Mukhopadhyay, A. *et al.* (2011) The interconversion of UDP-arabinopyranose and UDP-arabinofuranose is indispensable for plant development in Arabidopsis. *The Plant Cell*, **23**, 1373–1390.

Rennie, E.A. & Scheller, H.V. (2014) Xylan biosynthesis. *Current Opinion in Biotechnology*, **26**, 100–107.

Saulnier, L., Vigouroux, J. & Thibault, J.F. (1995) Isolation and partial characterization of feruloylated oligosaccharides from maize bran. *Carbohydrate Research*, **272**, 241–253.

Schendel, R.R., Meyer, M.R. & Bunzel, M. (2015) Quantitative profiling of feruloylated arabinoxylan side-chains from graminaceous cell walls. *Frontiers in Plant Science*, **6**, 1249.

Shao, W.C., Sharma, R., Clausen, M.H. & Scheller, H.V. (2020) Microscale thermophoresis as a powerful tool for screening glycosyltransferases involved in cell wall biosynthesis. *Plant Methods*, **16**.

Terrett, O.M. & Dupree, P. (2018) Covalent interactions between lignin and hemicelluloses in plant secondary cell walls. *Current Opinion in Biotechnology*, **56**, 97–104.

Tobimatsu, Y. & Schuetz, M. (2019) Lignin polymerization: how do plants manage the chemistry so well? *Current Opinion in Biotechnology*, **56**, 75–81.

Tryfona, T., Liang, H.C., Kotake, T., Tsumuraya, Y., Stephens, E. & Dupree, P. (2012) Structural characterization of Arabidopsis leaf arabinogalactan polysaccharides. *Plant Physiology*, **160**, 653–666.

Tryfona, T., Sorieul, M., Feijao, C., Stott, K., Rubtsov, D.V., Anders, N. *et al.* (2019) Development of an oligosaccharide library to characterise the structural variation in glucuronoarabinoxylan in the cell walls of vegetative tissues in grasses. *Biotechnology for Biofuels*, **12**, 109.

Vanholme, R., De Meester, B., Ralph, J. & Boerjan, W. (2019) Lignin biosynthesis and its integration into metabolism. *Current Opinion in Biotechnology*, **56**, 230–239.

Vogel, J. (2008) Unique aspects of the grass cell wall. *Current Opinion in Plant Biology*, **11**, 301–307.

Voiniciuc, C., Gunl, M., Schmidt, M.H. & Usadel, B. (2015) Highly Branched Xylan Made by IRREGULAR XYLEM14 and MUCILAGE-RELATED21 Links Mucilage to Arabidopsis Seeds. *Plant Physiology*, **169**, 2481–2495.

Waterstraat, M. & Bunzel, M. (2018) A Multi-step chromatographic approach to purify radically generated ferulate oligomers reveals naturally occurring 5–5/8-8(Cyclic)-,8–8(Noncyclic)/8-O-4-, and 5–5/8-8 (Noncyclic)-coupled dehydrotriferulic acids. *Front Chem*, **6**.

Wende, G. & Fry, S.C. (1997) O-feruloylated, O-acetylated oligosaccharides as side-chains of grass xylans. *Phytochemistry*, **44**, 1011–1018.

Zhong, R., Cui, D., Phillips, D.R. & Ye, Z.H. (2018) A Novel Rice Xylosyltransferase Catalyzes the Addition of 2-O-Xylosyl Side Chains onto the Xylan Backbone. *Plant and Cell Physiology*, **59**, 554–565.